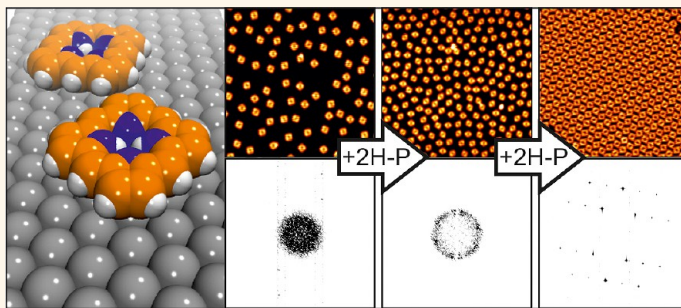


# How Surface Bonding and Repulsive Interactions Cause Phase Transformations: Ordering of a Prototype Macrocyclic Compound on Ag(111)

Felix Bischoff,<sup>†</sup> Knud Seufert,<sup>†</sup> Willi Auwärter,<sup>†,‡,\*</sup> Sushobhan Joshi,<sup>†</sup> Saranyan Vijayaraghavan,<sup>†</sup> David Écija,<sup>†</sup> Katharina Diller,<sup>†</sup> Anthoula C. Papageorgiou,<sup>†</sup> Sybille Fischer,<sup>†</sup> Francesco Allegretti,<sup>†</sup> David A. Duncan,<sup>†</sup> Florian Klappenberger,<sup>†</sup> Florian Blobner,<sup>†</sup> Runyuan Han,<sup>†</sup> and Johannes V. Barth<sup>†</sup>

<sup>†</sup>Physik Department E20, Technische Universität München, James Franck Straße 1, D-85748 Garching, Germany and <sup>‡</sup>Institute for Advanced Study, Technische Universität München, Lichtenbergstraße 2a, D-85748 Garching, Germany

## ABSTRACT



We investigated the surface bonding and ordering of free-base porphine (2H-P), the parent compound of all porphyrins, on a smooth noble metal support. Our multitechnique investigation reveals a surprisingly rich and complex behavior, including intramolecular proton switching, repulsive intermolecular interactions, and density-driven phase transformations. For small concentrations, molecular-level observations using low-temperature scanning tunneling microscopy clearly show the operation of repulsive interactions between 2H-P molecules in direct contact with the employed Ag(111) surface, preventing the formation of islands. An increase of the molecular coverage results in a continuous decrease of the average intermolecular distance, correlated with multiple phase transformations: the system evolves from an isotropic, gas-like configuration *via* a fluid-like phase to a crystalline structure, which finally gives way to a disordered layer. Herein, considerable site-specific molecule–substrate interactions, favoring an exclusive adsorption on bridge positions of the Ag(111) lattice, play an important role. Accordingly, the 2D assembly of 2H-P/Ag(111) layers is dictated by the balance between adsorption energy maximization while retaining a single adsorption site counteracted by the repulsive molecule–molecule interactions. The long-range repulsion is associated with a charge redistribution at the 2H-P/Ag(111) interface comprising a partial filling of the lowest unoccupied molecular orbital, resulting in long-range electrostatic interactions between the adsorbates. Indeed, 2H-P molecules in the second layer that are electronically only weakly coupled to the Ag substrate show no repulsive behavior, but form dense-packed islands.

**KEYWORDS:** porphyrin · porphine · repulsion · self-assembly · scanning tunneling microscopy · near-edge X-ray absorption fine structure · interface · photoelectron spectroscopy · charge transfer

In recent years much interest in the field of low-dimensional molecular nanostructures was focused on self-assembly protocols for surface-supported systems.<sup>1</sup> Thereby, organic molecules, programmed to engage in specific bonds with coadsorbates, represent a versatile library of functional tectons. The most common approach to engineer highly regular structures, also

offering a perspective for possible large-scale production, relies on *attractive* non-covalent intermolecular interactions, including van der Waals forces, hydrogen bonding, or metal coordination. A second strategy is to make use of competing repulsive and attractive forces to generate specific patterns deliberately.<sup>2–4</sup> Only lately have the first reports on the formation of long-range

\* Address correspondence to wilhelm.auwaerter@ph.tum.de.

Received for review November 26, 2012 and accepted March 13, 2013.

Published online March 22, 2013  
10.1021/nn305487c

© 2013 American Chemical Society

ordered structures *via* repulsive intermolecular forces emerged.<sup>5–9</sup> On the other hand, disordered systems based on dominating electrostatic or other repulsive interactions are well documented.<sup>10–14</sup>

A key feature of ordered assemblies stabilized by attractive interactions is the formation of regular arrangements at sub-monolayer coverage, due to the short-range character of the intermolecular forces. Consequently, a homogeneous structuring of a substrate, a frequent criterion for potential applications, is only achieved at saturation coverage and is in addition frequently hampered by the formation of multiple coexisting domains.<sup>15</sup> In contrast, with the exclusive presence of long-range repulsive interactions, molecules spread out over the entire available surface area in analogy to a two-dimensional lattice gas and the average intermolecular distance decreases continuously with increasing density. Thus, well-ordered high-coverage phases facilitate a homogeneous filling of the available surface without domain boundaries.<sup>5</sup> An additional advantage of repulsive systems that are often based on electrostatic forces induced by the charge redistribution at the sites of the molecules might be an electronic templating of the substrate.

Generally, structure formation and molecule–molecule interactions cannot be addressed without considering molecule–substrate interactions. The supporting surface not only offers a lattice of well-defined adsorption sites for the molecular tectons but might directly modify their conformational and electronic properties. This in turn affects the molecule–molecule interactions. For example, charge transfer or charge redistribution at the molecule/substrate interface can sensitively affect the self-assembly.<sup>2,16–20</sup>

Among molecules suitable for nanoarchitectures, porphyrins are considered as highly relevant tectons, given their manifold functions in biological systems and first successful implementations in artificial devices.<sup>21</sup> Consequently, it is currently of great interest to design novel porphyrin modules and to explore their potential for nanostructuring. This effort goes hand in hand with a fundamental characterization of porphyrins on surfaces, where the functional properties influenced by (i) the possible presence of a central metal ion, (ii) the substituents, and (iii) the conformation can be drastically modified upon adsorption.<sup>22–28</sup> To establish fundamental features of surface-anchored porphyrins and to clarify the influence of meso-substituents, it is mandatory to focus on the simplest possible system, which is the porphyrin macrocycle represented by the so-called free-base porphine (2H-P, Figure 1c).<sup>29,30</sup> Yet, not only is a detailed analysis of porphine adsorption on surfaces a prerequisite for the deeper understanding of more complex porphyrin systems, but 2H-P by itself is a very interesting module in the molecular construction kit for two- and three-dimensional nanoarchitectures.<sup>31</sup> Nonetheless,

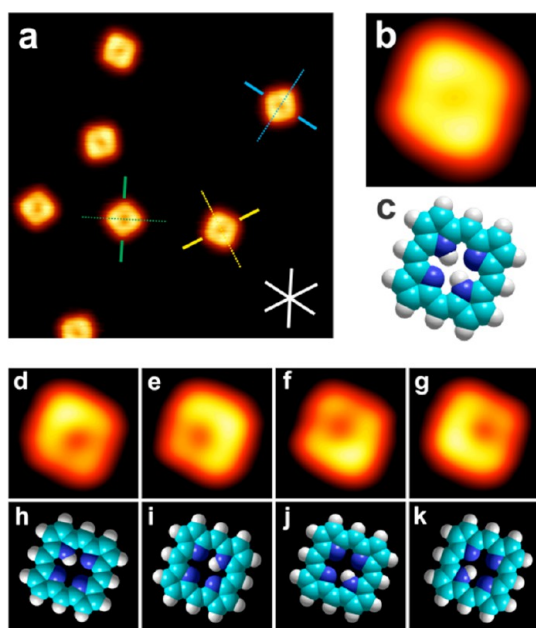


**Figure 1.** (a) Individual free-base porphines (2H-P) on Ag(111) exhibit three adsorption orientations rotated by  $\pm 60^\circ$  with respect to each other. The dotted colored lines mark the corresponding three directions of the molecular main axis (green, yellow, blue). The secondary molecular axes, which are aligned with the dense-packed  $\langle 1\bar{1}0 \rangle$  substrate directions (white star) are indicated by the solid lines ( $111 \times 111 \text{ \AA}^2 / t = 0.20 \text{ nA}$ ,  $U_B = -0.80 \text{ V}$ ). (b) Zoom-in: the orientations can be distinguished by a molecular main axis given by two protrusions above two corners of the square-like envelope ( $19 \times 19 \text{ \AA}^2$ ). (c) Model of 2H-P reflecting the orientation of the molecule in (b) (blue: nitrogen, cyan: carbon, white: hydrogen). (d) A controlled single-deprotonation procedure results in a 1H-P species. The remaining proton can be switched between the four nitrogen positions (d–g). The corresponding hydrogen configurations are represented in the models (h–k).

to date, knowledge on adsorbed 2H-P is essentially missing.<sup>30,31</sup>

This work presents a comprehensive characterization of free-base porphine, representing a prototype macrocyclic compound, on Ag(111) and reveals a surprisingly complex behavior of this model system, including phase transformations induced by repulsive interactions. The study focuses on the coverage-dependent ordering from sub-monolayer coverages up to the initial phase of second layer formation. It highlights the importance of site-specific interactions of the porphyrin macrocycle with the metal substrate and elucidates the crucial role of substitutional groups for low-dimensional self-assembly.

## RESULTS AND DISCUSSION

**Determination of Bonding Configuration and Site.** Typical scanning tunneling microscopy (STM) data of individual free-base porphines on Ag(111) are shown in Figure 1a,b. The molecules adsorb with the macrocycle plane aligned parallel to the surface and appear nearly square-like with a depression in the center. Since two corners are imaged brighter than the other two, the

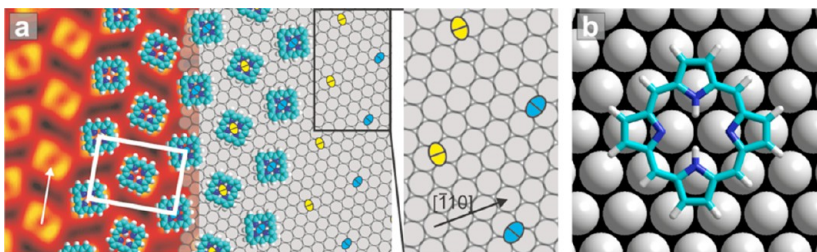


**Figure 2.** (a) Zoom-in STM image of the regular 2D lattice obtained at a coverage of 0.88 ML on the left ( $111 \times 88 \text{ \AA}^2 I_t = 0.17 \text{ nA}$ ,  $U_B = -0.35 \text{ V}$ ) and a model of the underlying Ag(111) surface on the right, both with a model overlay. The unit cell is indicated by a white rectangle; the white arrow points along the row direction characterized by molecules aligned in parallel. Centers of molecules with the same orientation are marked with yellow and blue ellipses. The ellipses' semimajor axes indicate the molecular main axis, and the semiminor axes indicate the secondary axis that is parallel to the high-symmetry axis of the substrate. The ellipses suggest bridge sites as the preferred adsorption sites. The panel on the right represents an enlarged model. (b) Structural model representing the adsorption of 2H-P on a bridge site of the Ag(111) lattice. This configuration is highly symmetric, as the nitrogen atoms and the meso-carbons are placed above Ag atoms.

molecules exhibit a 2-fold symmetry. These two brighter lobes in two opposing corners of the square define the molecular main axis (Figure 1a, dotted lines). A secondary axis is given by connecting the two dimmer corners (Figure 1a, solid lines). The images shown in Figure 1 were recorded at  $U_B = -0.8 \text{ V}$ , but porphines do not show significant voltage-dependent contrast, in accordance with featureless scanning tunneling spectra (*cf.* Figure S1 in the Supporting Information). At higher negative voltages ( $U_B < -2 \text{ V}$ ) the two lobes become slightly more prominent and the molecules have a rather rhombus-like outline. At high positive bias ( $U_B > 1 \text{ V}$ ) fewer details are resolved and the molecules appear as extended round protrusions. The two lobes of free-base porphine that define the main axis arise from an electronic effect induced by the position of the hydrogen pair bound to two of the inner nitrogens, as inferred from deprotonation and tautomerization experiments in analogy with 2H-TPP on Ag(111)<sup>32</sup> and 2H-Pc on Ag(111).<sup>33</sup> A voltage pulse of 2 V results in a controlled single deprotonation of the macrocycle and yields a 1H-P species (Figure 1d–g). Applying a procedure described in ref 32, the remaining single proton can be transferred between the four nitrogen sites, as visualized by the STM images in Figure 1d–g and the corresponding models (Figure 1h–k). Thereby, the position of the hydrogen defines the local conductance through the molecule, which thus represents a switch. This 1H-P four-position switch has a considerably smaller geometric footprint ( $\sim 1 \text{ nm}^2$ ) than the previously reported 2H-TPP module.<sup>32</sup>

The main axes of the molecules indicate different adsorption orientations on the Ag(111) lattice. For 2H-P, three adsorption orientations can be discriminated. Molecules are rotated by  $\pm(60 \pm 5)^\circ$  with respect to each other. We thus conclude that porphines adsorb with only one azimuthal orientation with respect to the dense-packed directions of the underlying surface, similar to tetrapyridylporphyrin (TPyP) on Cu(111)<sup>34</sup> and tetraphenylporphyrin (TPP) on Ag(111).<sup>35</sup>

To extract the exact adsorption site of 2H-P on Ag(111), we rely on a highly ordered 2H-P structure emerging at a coverage of 0.88 monolayer (ML) (Figure 2a). Here, one ML is defined as the highest experimentally observed molecular density on the surface before second layer growth starts (*vide infra*). This structure consists of parallel rows (along the arrow in Figure 2a), where the molecules in each row have the same adsorption orientation with a  $+30^\circ$  rotation against the row direction in one row and  $-30^\circ$  in the adjacent row, resulting in a  $60^\circ$  rotation between molecules in neighboring rows. The molecules within each row are equally separated by  $14.4 \pm 0.5 \text{ \AA}$ , thus revealing a clearly discernible intermolecular gap, and exhibit a center-to-center distance of  $12.3 \pm 0.5 \text{ \AA}$  to nearest neighbor molecules in the adjacent rows. These distances considerably exceed the smallest separation extracted from molecular mechanics simulations (MM<sup>+</sup>)<sup>36</sup> of  $11.1 \text{ \AA}$  for two 2H-Ps aligned in parallel and the nearest neighbor distance in the second layer ( $11.1 \text{ \AA}$ , *vide infra*). The structure therefore is not densely packed; that is, we observe intermolecular distances beyond van der Waals radii. The unit cell is centered rectangular and contains two molecules, as indicated in Figure 2a. A model overlay based on the experimental unit cell dimensions and the assumption of a single adsorption site reveals that 2H-P is centered on bridge sites with the secondary axis aligned parallel to the substrate's dense-packed  $\langle -1\bar{1}0 \rangle$  directions (Figure 2a). The model overlay is based on the experimental finding that extended domains without moiré patterns or other indications of an incommensurate registry are formed. Therefore the overlayer structure is considered commensurate, and every molecule with the same orientation should exhibit the same adsorption site, a condition only fulfilled for the bridge positions, and not for on-top or hollow sites. This configuration places the nitrogen and meso-carbon atoms above Ag atoms of the supporting surface (Figure 2b).

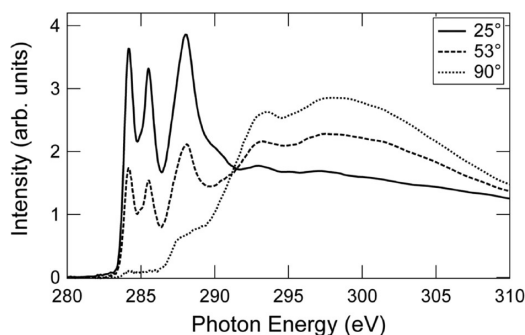


**Figure 3.** Angle-dependent C K-edge NEXAFS spectra of a sub-monolayer of 2H-P on Ag(111). The vanishing intensity of the  $1s \rightarrow \pi^*$  transition resonances in the  $90^\circ$  curve (dotted line) points to flat molecules that are adsorbed parallel to the Ag(111) surface.

In addition to the assembly shown in Figure 2a, we observed two rotational domains with a  $\pm 60^\circ$  rotated unit cell, as expected from the substrate symmetry. Consequently, the alignment and packing of the molecules is guided by the symmetry of the underlying Ag(111) surface.

The precise adsorption geometry of 2H-P/Ag(111), inaccessible to STM imaging, was determined by near-edge X-ray absorption fine structure (NEXAFS) spectroscopy recorded at three different angles of photon incidence. The intensity for a given transition depends on the angle between the linear polarization of the light and the direction of the final orbital.<sup>37</sup> By rotating the sample with respect to the beam, the incidence angle  $\theta$  between the E-vector of the X-ray beam and the surface normal can be varied. For an aromatic system like the free-base porphine, the intensity of the  $\pi^*$ -region is maximal for  $\theta = 0^\circ$  and minimal for  $\theta = 90^\circ$  if the molecule is adsorbed parallel to the surface.<sup>37,38</sup> Figure 3 shows the NEXAFS curves of a submonolayer of 2H-P taken at three different angles. The intensity of the peaks in the  $\pi^*$ -region (283–286 eV) vanishes for  $\theta = 90^\circ$  (dotted line), indicating planar molecules that adsorb parallel to the Ag(111) surface within the error bar of the setup ( $5^\circ$ ). The flat adsorption configuration is also consistent with the statement that the brighter protrusions of the main axis result from an electronic rather than a topographic effect. This corroborates the STM observations and discriminates 2H-P from its meso-substituted derivatives, like for example tetraphenylporphyrins, which experience major distortions upon adsorption on noble metal (111) surfaces.<sup>26,28,32</sup>

**Coverage-Dependent Assembly.** To get more insight into the assembly mechanism of 2H-P on Ag(111), different coverages ranging from 0.08 ML to a full ML were studied (Figure 4). Besides topographic STM images representing real space (Figure 4, a1–e1) a representative Fourier transformation (FT) plot is shown for each coverage (Figure 4, a2–e2). These FTs were generated using the fast FT function in the WSxM

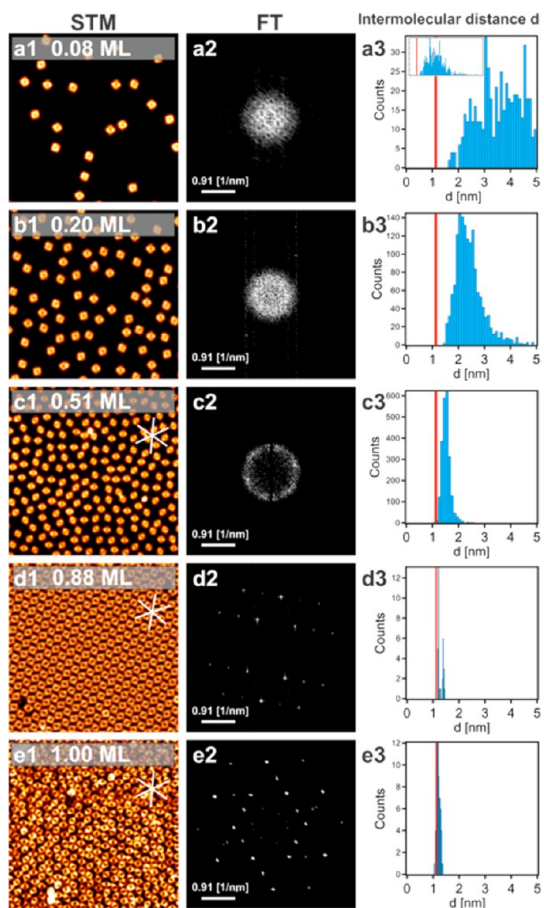


**Figure 4.** STM data of different molecular coverages of 2H-P on Ag(111) (column 1, (a1) 0.08 ML, (b1) 0.20 ML, (c1) 0.51 ML, (d1) 0.88 ML, (e1) 1 ML); FT images (column 2) and histograms of the intermolecular separations (column 3) corresponding to the coverages depicted in column 1. The porphine assemblies undergo three phase transformations from a lattice gas to a liquid-like phase (b  $\rightarrow$  c), from a liquid-like phase to a regular 2D lattice (c  $\rightarrow$  d), and finally from a regular lattice to a disordered layer (d  $\rightarrow$  e). The red line in the histograms represents the ideal intermolecular distance of 11.1 Å extracted from molecular mechanics calculations (MM<sup>+</sup>). All STM image sizes are  $221 \times 221 \text{ \AA}^2$ ; scanning conditions: (a1)  $I_t = 0.20 \text{ nA}$ ,  $U_B = -0.80 \text{ V}$ , (b1)  $I_t = 0.20 \text{ nA}$ ,  $U_B = -0.80 \text{ V}$ , (c1)  $I_t = 0.17 \text{ nA}$ ,  $U_B = -0.80 \text{ V}$ , (d1)  $I_t = 0.10 \text{ nA}$ ,  $U_B = -1.00 \text{ V}$ , (e1)  $I_t = 0.06 \text{ nA}$ ,  $U_B = -0.30 \text{ V}$ .

software.<sup>39</sup> In addition, the intermolecular separations were extracted from the STM images for all coverages. The histograms representing the distances from every molecule to its three closest neighbors (Figure 4, a3–e3) were obtained by binning hundreds of intermolecular distances with a bin width of 1 Å (0.25 Å in Figure 4d3 and 4e3).

At coverages below 0.88 ML porphines are distributed over the entire surface and appear as a dispersed system of particles with a broad distribution of intermolecular distances (Figure 4a–c). Despite a preparation temperature of 340 K, guaranteeing a considerable molecular mobility, and the subsequent slow cooling to cryogenic temperatures, no agglomerates, dimers, or ordered structures are present. Porphines apparently

interact repulsively and exhibit a barrier for dimer formation, which prevents self-assembly.

With increasing coverage and less free area on the surface the porphines are forced to approach each other, and spatial restrictions allow less variation in the intermolecular separations. The distance distribution shifts to smaller distances and gets narrower (Figure 4a3, b3, c3).

The coverage-dependent ordering is also reflected in the evolution of the FT of STM images representing increasing density. At first an isotropic, diffuse disk is visible (Figure 4a2) that changes to a blurry ring (Figure 4b2), which sharpens with increasing coverage and comprises six spots forming a hexagon (Figure 4c2). It then transforms to a defined face-centered rectangular pattern (Figure 4d2), which finally evolves into a pattern with hexagonal symmetry (Figure 4e2). Throughout the full coverage range, the distances within the FT plots increase; that is, the intermolecular distances continuously decrease.

The different FT patterns can be explained by simply considering repulsive effects in combination with the influence of the substrate. A dispersed system would give just a smooth, featureless background in the FT (Figure 4a2). In general, a ring arises from lower and upper restrictions to the distribution. Here, the lower limit for the porphine separations is provided by short-range repulsive molecule–molecule interactions, while the coverage gives an upper limit. At all coverages each porphine tries to maximize its distance to all neighbors in order to minimize its potential energy in the repulsive interaction. Consequently, the multiple interactions lead to a preferred intermolecular distance (Figure 4b2). The resulting distribution is isotropic and resembles a snapshot of a molecular gas phase. At higher coverage, the bright spots in a hexagonal arrangement superimposed on the ring (Figure 4c2) indicate of a short-range order between molecules. We associate this change from a dispersed system (essentially isotropic distribution) to a system with defined relations between neighboring molecules (anisotropic distribution) with a transformation from a gas to liquid-like state. The origin of the anisotropy and therefore the aforescribed phase transformation is most likely substrate induced, since the orientation of the hexagonal spots is linked to the substrate geometry, irrespective of coverage or sample preparation.

The reduced disorder evidenced by the sharp FT patterns at higher coverages (Figure 4d2, e2) is also reflected in the distance distribution, which evolves *via* an intermediate step exhibiting two pronounced peaks representing the highly ordered structure (Figure 4d3) into a narrow peak representing a mean separation of 12.1 Å (Figure 4e3). The distributions for these two highest coverages are extremely narrow, which is characteristic for a crystalline structure.

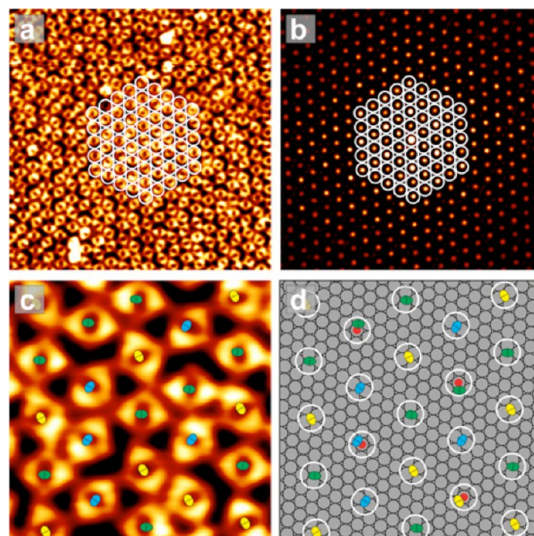


**Figure 5. Quasi-hexagonal 1 ML structure.** (a) Typical STM image ( $221 \times 221 \text{ \AA}^2$ ,  $I_t = 0.06 \text{ nA}$ ,  $U_B = -0.30 \text{ V}$ ) and (b) the corresponding autocorrelation plot with a hexagonal grid that fits the detected periodicity well. (c) Zoom-in image highlighting the positional and rotational disorder in the structure. (d) Model representing the assembly in (c). White circles mark the nodes of the regular hexagonal grid, which include unfavorable “on top” adsorption sites (red dots). Their avoidance induces a disordered character to the layer (compare Figure 2).

Indeed porphines form a highly ordered 2D lattice at 0.88 ML, as discussed in the previous section, but the final 1 ML structure cannot be considered as a crystal with translational symmetry. It does not feature strict positional order, and it lacks orientational order.

This reduced regularity is evidenced by the STM image represented in Figure 5a. The corresponding autocorrelation plot (Figure 5b) reveals a hexagonal symmetry with a periodicity of  $12.1 \pm 0.5 \text{ \AA}$ . But a superposition of this hexagonal lattice with the STM data (Figure 5a) clearly shows that the full monolayer is not highly ordered. The molecules show no fixed orientation relative to their nearest neighbors, and the centers of the molecules deviate slightly from a perfect hexagonal arrangement. The structure has only an average positional but no orientational order and is therefore considered a disordered layer.<sup>40</sup> To rationalize this observation, we extracted the molecular positions from a high-resolution STM image (Figure 5c) and superimposed them on a structural model of the Ag(111) surface together with a perfect hexagonal grid with a periodicity of 12.35 Å, symbolized by the white circles (Figure 5d). Thereto, the Ag(111) substrate was aligned with the molecular secondary axis. The 2H-P molecules arranged in such a hexagonal lattice cannot occupy solely bridge sites, but one out of four positions coincides with an “on top” site (red dots), which is an unfavored adsorption geometry. Consequently, molecules avoid “on top” sites and evade to one of the six adjacent bridge positions. Therefore, the molecular

arrangement deviates from a perfect hexagonal lattice and does not show orientational order. In addition, the average defect density observed in the experiments exceeds the 25% suggested by the local model overlay of the lattice. Accordingly we are not dealing with a well-ordered lattice, but rather with a disordered layer in the sense that the position of a considerable fraction of the molecules is randomly assigned to one out of the six possibilities, resulting in three possible orientations (marked in green, yellow, and blue in Figure 5d).

The idealized hexagonal grid (Figure 5d) is rotated by 6° with respect to the dense-packed directions of the Ag(111) substrate and presents a periodicity of 12.35 Å. These values are in perfect agreement with the lattice derived from LEED and STM observations of a 1 ML NiP on Ag(111)<sup>41</sup> and on Ag/Si(111)-(√3 × √3)R30°.<sup>42</sup> In both cases NiP is reported to form hexagonal densely packed islands with positional and orientational order. However the pertaining STM data lack intramolecular resolution and the experiments were carried out at room temperature, where NiP molecules are quite mobile; that is, it is possible that the seemingly orientational order is a dynamic feature reflecting continuous molecular motion.

In the following, we will apply energetic considerations combined with the observation of a single adsorption site of 2H-P on Ag(111) to rationalize the intermolecular distance decrease, the formation of the crystalline structure, and the transformation to the disordered layer. Our findings evidence that the increase in total adsorption energy at higher coverages, given simply by the larger number of molecules per surface area, outweighs the stronger repulsion induced by smaller separations between the molecules, which results in a decrease of the observed intermolecular distances. During this compression molecules rearrange laterally and rotationally. However, this adaptation is limited by molecule–substrate interactions that steer the porphines into one of the three equivalent adsorption orientations, irrespective of coverage. At 0.88 ML the maximum number of preferred adsorption sites coincides with a regular lattice, whereby this structure is highly ordered, but obviously not densely packed. At coverages exceeding 0.88 ML, molecules can occupy only the preferred adsorption sites by abandoning the order of the structure and consequently form a disordered layer, as defined above. However, even the resulting layer is not densely packed. The variations in the adsorption configurations within the hexagonal structure show that some molecules had enough clearance for rotation and/or translation. Nevertheless the structure is not compressed upon deposition of additional molecules, but second layer growth begins (*vide infra*). Apparently, the energy penalty given by the repulsive interactions at very small

intermolecular distances cannot be compensated by the gain in adsorption energy or attractive short-range forces. Therefore, molecule–substrate interactions that induce specific adsorption sites appear to be decisive for the 2H-P arrangement on Ag(111). The ordering is coverage dependent, *i.e.*, density-driven, and reflects the symmetry of the underlying substrate.

It is instructive to compare our FT with low-energy electron diffraction (LEED) patterns reported in the literature for related systems dominated by repulsive molecule–molecule interactions.<sup>5,6,8,9,43</sup> Both observations map reciprocal space and evidence structural transformations with increasing molecular coverage. The evolution of the LEED diffraction patterns shows a strikingly similar behavior as the FT plots for 2H-P/Ag(111): The LEED experiments for the series of systems evidence phase transformations from a disordered gas-like phase (diffuse disk) to a liquid-like phase with noticeable short-range order (ring with spots) to a relaxed solid structure (first sharp pattern, analogous to the presented regular lattice at 0.88 ML) to a final dense-packed solid structure (second sharp pattern, analogous to the quasi-hexagonal disordered layer at 1 ML).<sup>8</sup> Thus, the described coverage-dependent transformations seem to represent a quite general characteristic featuring free energy minimization regardless of the specific applied tecton or substrate. Even surface-supported alkali metal layers evidence analogous phases and transformations.<sup>44–46</sup> However, one fundamental issue discriminates the 2H-P/Ag(111) system from the previous reports. Even at the highest density, we do not observe an orientationally and positionally ordered structure formed at the expense of incommensurate adsorption sites or a tilting of the molecules. Thus, site-specific molecule–substrate interactions are clearly more important for 2H-P/Ag(111) than for the previously described systems, where the maximization of the total adsorption energy can even outweigh the energy penalty caused by deviations from ideal adsorption sites.

**Second Layer Assembly.** Additional molecule deposition onto the disordered quasi-hexagonal 1 ML structure does not result in a further compression of the intermolecular distances, but induces second layer formation. Figure 6 shows an STM image of a coverage exceeding 1 ML exhibiting ordered two-dimensional islands with an apparent height clearly exceeding the first layer molecules. Molecules within the islands appear as cloverleaf-shaped protrusions presenting a single orientation (Figure 6). This modified appearance compared to the surrounding porphines in direct contact with the Ag(111) surface points to a reduced electronic coupling in line with previous reports on second layer molecules.<sup>47–49</sup> The resulting assembly is characterized by a rhombic unit cell with side lengths

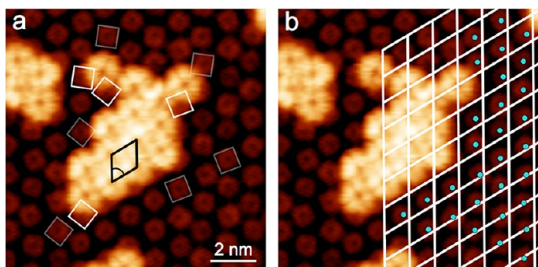


**Figure 6.** Initial phase of second layer growth of 2H-P on Ag(111). The second layer porphines appear as cloverleaf-shaped protrusions exhibiting an identical orientation within each island. (a) At the island border, subjacent first layer molecules are partially discernible (outlined by white squares). The rhombic unit cell is marked by the black diamond ( $I_t = 20$  pA,  $U_B = 2$  V). (b) The lattice formed by the second layer molecules (white grid) is not in registry with the surrounding quasi-hexagonal pattern of the first layer molecules (blue dots).

of  $12.3 \pm 0.7$  Å and  $11.1 \pm 0.7$  Å and an opening angle of  $57 \pm 5^\circ$  (Figure 6a). This packing leads to incommensurability with respect to the quasi-hexagonal first layer (Figure 6b), as also directly inferred from the joint imaging of first and second layer molecules at the border of the islands outlined in Figure 6a. This observation also proves that the bright molecules are indeed second layer molecules placed on first layer molecules and not tilted species still in direct contact with the Ag(111) substrate. Consequently, the molecular arrangement in the second layer is not dominated by preferred adsorption sites on the disordered first layer, but rather by lateral intermolecular interactions (Figure 6b). Here, it is important to note that the 2H-P molecules in the second layer readily self-assemble into dense-packed islands, which can extend to a full layer, in striking contrast to the 2H-P in direct contact with the Ag(111) surface, which interact repulsively. Consequently, molecule–substrate interactions seem to induce the repulsive behavior.

**Discussion.** We now discuss possible origins of the repulsive behavior observed for the (sub-)ML coverage regime. Repulsive interactions resulting in individual adsorbates on surfaces are reported for a variety of systems. The driving mechanisms inducing the separation of adatoms or molecules are diverse and include surface state mediated effects,<sup>50–53</sup> entropy,<sup>54</sup> strain,<sup>55–57</sup> and dipole interactions due to charge transfer<sup>58</sup> or the push-back effect.<sup>8</sup> Most of these effects can be ruled out as the dominant contribution to the apparent repulsion in the 2H-P/Ag(111) case: (i) Friedel oscillations in the surface state electron density are reported to induce a barrier for dimer formation for atomic adsorbates<sup>50–52</sup> and yield maxima in the interatomic distance distribution spaced by half the Fermi wavelength ( $\lambda_F/2$ ) of the surface state electrons. An inspection of the intermolecular separations of 2H-P (Figures 4a3–e3) however suggests otherwise.

First of all, the pair distributions do not show maxima separated by multiples of  $\lambda_F/2$ , where  $\lambda_F/2$  equals 3.8 nm for Ag(111),<sup>51,59</sup> and second, the preferred distance is coverage dependent. (ii) Recent reports suggest that entropy might counteract the self-assembly of well-ordered molecular structures and thus favor a random distribution of adsorbates, mimicking a repulsive interaction.<sup>54</sup> Yet, in such a situation one expects to find some molecules in close contact, even at low and intermediate coverages.<sup>11</sup> As this is not the case for 2H-P/Ag(111), we exclude a “maximization of disorder” as the driving force for the dispersed distribution of individual molecules on the surface. However, it should be pointed out that the identification of “maximal entropy” with “lowest order” in a system is not generally valid.<sup>11,60</sup> (iii) Another potential source for individual adsorbates is elastic deformations of the substrate causing strain fields and strain relief patterns that might induce analogous consequences as electrostatic interactions<sup>61</sup> and lead to repulsive forces between adsorbates. If heteroepitaxial films are used, strain effects can indeed be important.<sup>56,57</sup> This is not the case for unreconstructed single crystal surfaces such as Ag(111). Here, strain can be induced by adsorbed atoms or molecules,<sup>55,62,63</sup> and such elastic deformations might contribute to molecule–molecule interactions, but are not reported to play an important role for large organic molecules. (iv) Repulsive dipole–dipole interactions leading to a disordered phase are known for polar molecules that adsorb in the same orientation onto the surface,<sup>10</sup> but are also reported for intrinsically nonpolar molecules.<sup>58</sup> For the latter, a dipole moment perpendicular to the surface plane can be induced upon adsorption, caused by charge transfer between adsorbate and surface and/or by the push-back effect. Indeed charge transfer is reported for many organic molecules on metal surfaces, including porphines.<sup>30,38,64</sup> The charge redistribution at the porphine/metal interface due to hybridization results for example in a partial filling of the lowest unoccupied orbital (LUMO) of 2H-P chemisorbed on Cu(110).<sup>30</sup>

In fact, for the 2H-P/Ag(111) system, ultraviolet photoelectron spectroscopy (UPS) measurements summarized in Figure 7 evidence a charge transfer to the porphine. The spectral feature right below the Fermi level represents the occupied tail of the LUMO orbital, indicating a downshift and partial filling of this orbital.<sup>65,66</sup> By subtracting the Ag(111) from the 2H-P/Ag(111) spectrum (black curve in Figure 7a), we estimate the occupation of the LUMO to be about 10% of the HOMO-related feature. This is consistent with our complementary NEXAFS measurements, which rule out a massive charge transfer and a complete filling of the LUMO (see Supporting Information, Figure S2). Moreover, the contrast revealed by STM images representing occupied electronic states recorded with a tip

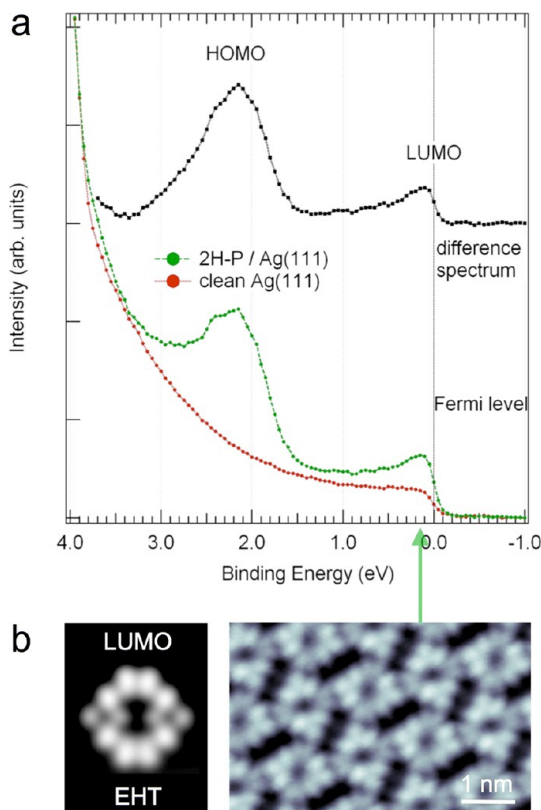


**Figure 7. Charge transfer to the LUMO.** (a) Photoemission spectra comparing the valence band region of 2H-P/Ag(111) (in green) at a coverage close to the monolayer to the bare Ag(111) (in red). The data clearly show the signature of the highest occupied molecular orbital (HOMO) of porphine at a binding energy of about 2.2 eV. More importantly, the intensity increase right below the Fermi level represents a partial filling of the LUMO upon adsorption on Ag(111). From the difference spectrum (in black, vertically offset for clarity) we estimate the occupation of the LUMO to be about 10% of the HOMO; that is, the LUMO remains mainly unoccupied, in agreement with the NEXAFS data (see Supporting Information, Figure S2) (Photon energy: 30 eV, emission: 60° off-normal). (b) The symmetry and nodal structure of a calculated constant charge density contour representing the LUMO of an isolated 2H-P (left panel, extended Hückel theory (EHT)) shows a close resemblance to high-resolution STM images representing occupied states (right panel,  $I_t = 0.2$  nA,  $U_B = -0.15$  V).

yielding high spatial resolution (Figure 7b right) closely resembles the nodal structure of the LUMO (see Figure 7b left), thus corroborating a charge transfer into this orbital.

Based on these arguments, a charge redistribution at the 2H-P/Ag(111) interface comprising a partial filling of the LUMO orbital is the most likely origin of the repulsive interaction, which exceeds attractive forces.

## CONCLUSIONS

In summary, we applied STM, UPS, and NEXAFS spectroscopy to characterize the adsorption of 2H-P on Ag(111) from 0.08 ML up to the initial stage of second layer growth. 2H-Ps occupy exclusively bridge positions on the Ag(111) lattice. This indicates that considerable site-specific molecule–substrate interactions

are operative. In addition, the analysis of intermolecular distances reveals a repulsive interaction between the 2H-P molecules inducing an energy barrier for aggregation that prevents supramolecular self-assembly. These two characteristics, *i.e.*, the preferred adsorption sites and the repulsive interaction, dictate the 2H-P morphology on Ag(111) throughout the coverage range up to 1 ML. During the continuous decrease of the average intermolecular distance, multiple phase transformations take place. At very low coverage, individual 2H-Ps representing an isotropic lattice gas are resolved. Around 0.5 ML a transformation to an anisotropic fluid-like phase is observed. At 0.88 ML a special condition is fulfilled: The intermolecular distances fit to a lattice only comprising the preferred bridge adsorption sites with well-defined azimuthal orientations between neighboring molecules. As a result, a highly ordered, crystal-like structure is observed. Importantly, this assembly is not dense-packed, and attractive intermolecular interactions do not seem to play a relevant role. At higher coverages, porphines can adsorb on the surface only by disrupting the order of the structure. Thus, we observe the transformation to a disordered layer, exhibiting an average hexagonal but no strict orientational order. This final structure, defined as 1 ML even if not dense-packed, represents the highest packing density of 2H-P observed on Ag(111). Further porphine deposition induces the assembly of compact second layer islands.

Our experimental observations suggest that the assembly of 2H-P/Ag(111) is driven by the maximization of the adsorption energy considering the boundary conditions given by the repulsive molecule–molecule interactions and the single adsorption sites. The repulsion is assigned to a charge redistribution at the 2H-P/Ag(111) interface comprising a partial filling of the LUMO, resulting in adsorption-induced dipole moments perpendicular to the surface plane. Indeed, the second layer 2H-P molecules that are electronically only weakly coupled to the metallic substrate show no repulsive behavior, but rather form dense-packed islands.

Compared to other adsorbate structures driven by nonattractive and repulsive forces, 2H-P on Ag(111) is special in the sense that the balance of molecule–molecule and molecule–substrate interactions prevents the formation of incommensurate layers at high coverage. Even more importantly, 2H-P, representing the macrocyclic parent compound of all porphyrins, behaves completely different from its free-base tetraphenylporphyrin counterpart (2H-TPP) or related metalloporphyrins (M-TPP), which all form highly ordered dense-packed arrays on Ag(111) even at sub-monolayer coverage.<sup>28,32,35,67</sup> This evidences the importance of the terminal substituents for a successful self-assembly *via* decoupling from the substrate or

attractive interactions. In striking contrast to its meso-substituted derivatives, the 2H-P/Ag(111) sys-

tem reveals a wide variety of surface structures and phases.

## METHODS

All STM experiments were performed in a custom-designed ultrahigh-vacuum chamber housing a CreaTec STM operated at 6 K ([www.lt-stm.com](http://www.lt-stm.com)). The base pressure during the experiments was around  $2 \times 10^{-10}$  mbar. Repeated cycles of Ar<sup>+</sup> sputtering and annealing to 725 K were used to prepare the Ag(111) single crystal. Subsequently 2H-P molecules (Frontier Scientific, purity >95%) were dosed from a thoroughly degassed quartz crucible held at 470 K. During deposition the sample was kept at 340 K. All STM images were recorded in constant current mode using an electrochemically etched tungsten tip prepared by sputtering and controlled dipping into the Ag(111) substrate. In the figure captions  $U_B$  refers to the bias voltage applied to the sample. The WSxM program ([www.nanotec.es](http://www.nanotec.es)) was used to display the STM images.<sup>39</sup>

The NEXAFS data were taken at the HE-SGM beamline at BESSY II in Berlin using the partial electron yield mode with a retarding voltage of 150 V. The sample preparation followed the recipe introduced in the paper. The spectra were recorded at a sample temperature of 125 K. Data collection and analysis followed the procedure described in ref 38. The UPS measurements were conducted at the Materials Science beamline of the ELETTRA synchrotron facility in Trieste, Italy. The end station consists of a typical UHV surface science chamber, equipped with facilities for sample manipulation and characterization, and operated at a base pressure of  $2 \times 10^{-10}$  mbar. All measurements were performed with the sample kept at room temperature, using a SPECS PHOIBOS 150 electron energy analyzer of 150 mm mean radius with a nine-channel detector. Linearly polarized radiation with photon energies in the range 22–120 eV was used, and the electron collection geometry was varied between normal and grazing emission (60° off-normal, corresponding to normal incidence of the photon beam) with an acceptance angle of  $\pm 7^\circ$ . The energy resolution, mainly determined by the chosen pass energy of the analyzer, was approximately 0.13 eV. The UPS measurements were complemented by X-ray photoelectron spectroscopy (XPS) and NEXAFS data, in order to verify the cleanliness, chemical state, coverage, and molecular orientation in the as-prepared layers.

**Conflict of Interest:** The authors declare no competing financial interest.

**Acknowledgment.** We thank R. G. Acres and K. C. Prince for beamtime support and organization. Experimental assistance of P. Feulner is gratefully acknowledged. Work was supported by the ERC Advanced Grant MolArt (no. 247299), the German Research Foundation (DFG) through BA 3395/2-1, the Munich Center for Advanced Photonics (MAP), and the Technische Universität München, Institute for Advanced Study, funded by the German Excellence Initiative. A.C.P. was supported by a Marie Curie Intra-European Fellowship (project NASUMeca, no. 274842). We thank the Helmholtz-Zentrum Berlin, Electron Storage Ring BESSY II, for provision of synchrotron radiation at beamline HE-SGM. Traveling costs for the BESSY measurements provided by Helmholtz-Zentrum Berlin are gratefully acknowledged.

**Supporting Information Available:** Scanning tunneling spectroscopy on 2H-P/Ag(111). NEXAFS comparison of 2H-P multi- and monolayer on Ag(111). This material is available free of charge via the Internet at <http://pubs.acs.org>.

## REFERENCES AND NOTES

- Barth, J. V. Molecular Architectonic on Metal Surfaces. *Annu. Rev. Phys. Chem.* **2007**, *58*, 375–407.
- Tomba, G.; M., S.; Schneider, W.-D.; Baldereschi, A.; De Vita, A. Supramolecular Self-Assembly Driven by Electrostatic Repulsion: The 1D Aggregation of Rubrene Pentagons on Au(111). *ACS Nano* **2010**, *4*, 7545–7551.
- Fraxedas, J.; Garcia-Gil, S.; Monturet, S.; Lorente, N.; Fernandez-Torrente, I.; Franke, K. J.; Pascual, J. I.; Vollmer, A.; Blum, R.-P.; Koch, N.; et al. Modulation of Surface Charge Transfer through Competing Long-Range Repulsive versus Short-Range Attractive Interactions. *J. Phys. Chem. C* **2011**, *115*, 18640–18648.
- Pennec, Y.; Auwärter, W.; Schiffrian, A.; Weber-Bargioni, A.; Riemann, A.; Barth, J. V. Supramolecular Gratings for Tunable Confinement of Electrons on Metal Surfaces. *Nat. Nanotechnol.* **2007**, *2*, 99–103.
- Stadler, C.; Hansen, S.; Kröger, I.; Kumpf, C.; Umbach, E. Tuning Intermolecular Interaction in Long-Range-Ordered Submonolayer Organic Films. *Nat. Phys.* **2009**, *5*, 153–158.
- Kröger, I.; Stadtmüller, B.; Stadler, C.; Ziroff, J.; Kochler, M.; Stahl, A.; Pollinger, F.; Lee, T.-L.; Zegenhagen, J.; Reinert, F.; et al. Submonolayer Growth of Copper-Phthalocyanine on Ag(111). *New J. Phys.* **2010**, *12*, 083038.
- Fernandez-Torrente, I.; Monturet, S.; Franke, K. J.; Fraxedas, J.; Lorente, N.; Pascual, J. I. Long-Range Repulsive Interaction between Molecules on a Metal Surface Induced by Charge Transfer. *Phys. Rev. Lett.* **2007**, *99*, 176103–176103.
- Wagner, C.; Kasemann, D.; Golnik, C.; Forker, R.; Esslinger, M.; Müllen, K.; Fritz, T. Repulsion between Molecules on a Metal: Monolayers and Submonolayers of Hexa-Peri-Hexabenzocoronene on Au(111). *Phys. Rev. B* **2010**, *81*, 035423–035423.
- Seidel, C.; Ellerbrake, R.; Gross, L.; Fuchs, H. Structural Transitions of Perylene and Coronene on Silver and Gold Surfaces: A Molecular-Beam Epitaxy Leed Study. *Phys. Rev. B* **2001**, *64*, 195418–195418.
- Yokoyama, T.; Takahashi, T.; Shinozaki, K.; Okamoto, M. Quantitative Analysis of Long-Range Interactions between Adsorbed Dipolar Molecules on Cu(111). *Phys. Rev. Lett.* **2007**, *98*, 206102–206102.
- Soubatch, S.; Kröger, I.; Kumpf, C.; Tautz, F. S. Structure and Growth of Tetracene on Ag(111). *Phys. Rev. B* **2011**, *84*, 195440.
- Rojas, G.; Chen, X.; Bravo, C.; Kim, J.-H.; Kim, J.-S.; Xiao, J.; Dowben, P. A.; Gao, Y.; Cheng Zeng, X.; Choe, W.; et al. Self-Assembly and Properties of Nonmetalated Tetraphenyl-Porphyrin on Metal Substrates. *J. Phys. Chem. C* **2010**, *114*, 9408–9415.
- Buchner, F.; Zillner, E.; Röckert, M.; Gläsel, S.; Steinrück, H.-P.; Marbach, H. Substrate-Mediated Phase Separation of Two Porphyrin Derivatives on Cu(111). *Chem.—Eur. J.* **2011**, *17*, 10226–10229.
- Rojas, G.; Simpson, S.; Chen, X.; Kunkel, D. A.; Nitz, J.; Xiao, J.; Dowben, P. A.; Zurek, E.; Enders, A. Surface State Engineering of Molecule-Molecule Interactions. *Phys. Chem. Chem. Phys.* **2012**, *14*, 4971–4976.
- Kühne, D.; Klappenberger, F.; Decker, R.; Schlickum, U.; Brune, H.; Klyatskaya, S.; Ruben, M.; Barth, J. V. Self-Assembly of Nanoporous Chiral Networks with Varying Symmetry from Sexiphenyl-Dicarbonitrile on Ag(111). *J. Phys. Chem. C* **2009**, *113*, 17851–17859.
- Vaughan, O. P. H.; Alavi, A.; Williams, F. J.; Lambert, R. M. Dipole Amplification: A Principle for the Self-Assembly of Asymmetric Monomers on Metal Surfaces. *Angew. Chem., Int. Ed.* **2008**, *47*, 2422–2426.
- Papageorgiou, A. C.; Alavi, A.; Lambert, R. M. Self-Assembly at Room Temperature of Thermally Stable Discrete and Extended Oligomers of Polycyclic Aromatics on Ag(110): Induced Dipoles and Cooperative Effects. *Chem. Commun.* **2012**, *48*, 3394–3396.
- Jewell, A. D.; Simpson, S. M.; Enders, A.; Zurek, E.; Sykes, E. C. H. Magic Electet Clusters of 4-Fluorosyrene on Metal Surfaces. *J. Phys. Chem. Lett.* **2012**, *3*, 2069–2075.

19. Han, P.; Weiss, P. S. Electronic Substrate-Mediated Interactions. *Surf. Sci. Rep.* **2012**, *67*, 19–81.
20. Tseng, T.-C.; Urban, C.; Wang, Y.; Otero, R.; Tait, S. L.; Alcamí, M.; Ecija, D.; Trelika, M.; Gallego, J. M.; Lin, N.; et al. Charge-Transfer-Induced Structural Rearrangements at Both Sides of Organic/Metal Interfaces. *Nat. Chem.* **2010**, *2*, 374–379.
21. Mohnani, S.; Bonifazi, D. Supramolecular Architectures of Porphyrins on Surfaces: The Structural Evolution from 1D to 2D to 3D to Devices. *Coord. Chem. Rev.* **2010**, *254*, 2342–2362.
22. Bernien, M.; Miguel, J.; Weis, C.; Ali, M. E.; Kurde, J.; Krumme, B.; Panchmatia, P. M.; Sanyal, B.; Piatek, M.; Srivastava, P.; et al. Tailoring the Nature of Magnetic Coupling of Fe-Porphyrin Molecules to Ferromagnetic Substrates. *Phys. Rev. Lett.* **2009**, *102*, 047202.
23. Donovan, P.; Robin, A.; Dyer, M.; Persson, M.; Raval, R. Unexpected Deformations Induced by Surface Interaction and Chiral Self-Assembly of Co<sup>II</sup>-Tetraphenylporphyrin (Co-TPP) Adsorbed on Cu(110): A Combined STM and Periodic DFT Study. *Chem.—Eur. J.* **2010**, *16*, 11498.
24. Jung, T. A.; Schlittler, R. R.; Gimzewski, J. K. Conformational Identification of Individual Adsorbed Molecules with the STM. *Nature* **1997**, *386*, 696.
25. Scudiero, L.; Barlow, D. E.; Mazur, U.; Hipp, K. W. Scanning Tunneling Microscopy, Orbital-Mediated Tunneling Spectroscopy, and Ultraviolet Photoelectron Spectroscopy of Metal(II) Tetraphenylporphyrins Deposited from Vapor. *J. Am. Chem. Soc.* **2001**, *123*, 4073–4080.
26. Yokoyama, T.; Yokoyama, S.; Kamikado, T.; Mashiko, S. Nonplanar Adsorption and Orientational Ordering of Porphyrin Molecules on Au(111). *J. Chem. Phys.* **2001**, *115*, 3814.
27. Auwärter, W.; Klappenberger, F.; Weber-Bargioni, A.; Schiffirin, A.; Strunkus, T.; Wöll, C.; Pennec, Y.; Riemann, A.; Barth, J. V. Conformational Adaptation and Selective Adatom Capturing of Tetraphenylporphyrin Molecules on a Copper (111) Surface. *J. Am. Chem. Soc.* **2007**, *129*, 11279–11285.
28. Auwärter, W.; Seufert, K.; Klappenberger, F.; Reichert, J.; Weber-Bargioni, A.; Verdini, A.; Cvetko, D.; Dell'Angela, M.; Floreano, L.; Cossaro, A.; et al. Site-Specific Electronic and Geometric Interface Structure of Co-Tetraphenylporphyrin Layers on Ag(111). *Phys. Rev. B* **2010**, *81*, 245403–245403.
29. Webb, L. E.; Fleischer, E. B. Crystal Structure of Porphine. *J. Chem. Phys.* **1965**, *43*, 3100–3111.
30. Dyer, M. S.; Robin, A.; Haq, S.; Raval, R.; Persson, M.; Klimes, J. i., Understanding the Interaction of the Porphyrin Macrocycle to Reactive Metal Substrates: Structure, Bonding, and Adatom Capture. *ACS Nano* **2011**, *5*, 1831–1838.
31. Haq, S.; Hanke, F.; Dyer, M. S.; Persson, M.; Iavicoli, P.; Amabilino, D. B.; Raval, R. Clean Coupling of Unfunctionalized Porphyrins at Surfaces to Give Highly Oriented Organometallic Oligomers. *J. Am. Chem. Soc.* **2011**, *133*, 12031–12039.
32. Auwärter, W.; Seufert, K.; Bischoff, F.; Ecija, D.; Vijayaraghavan, S.; Joshi, S.; Klappenberger, F.; Samudrala, N.; Barth, J. V.; Surface-Anchored, A. Molecular Four-Level Conductance Switch Based on Single Proton Transfer. *Nat. Nanotechnol.* **2012**, *7*, 41–46.
33. Sperl, A.; Kröger, J.; Berndt, R. Controlled Metalation of a Single Adsorbed Phthalocyanine. *Angew. Chem., Int. Ed.* **2011**, *50*, 5294–5297.
34. Klappenberger, F.; Weber-Bargioni, A.; Auwärter, W.; Marschall, M.; Schiffirin, A.; Barth, J. V. Temperature Dependence of Conformation, Chemical State, and Metal-Directed Assembly of Tetraphenylporphyrin on Cu(111). *J. Chem. Phys.* **2008**, *129*.
35. Auwärter, W.; Weber-Bargioni, A.; Brink, S.; Riemann, A.; Schiffirin, A.; Ruben, M.; Barth, J. V. Controlled Metalation of Self-Assembled Porphyrin Nanoarrays in Two Dimensions. *ChemPhysChem* **2007**, *8*, 250–254.
36. HyperChem(TM), Hypercube, Inc., 1115 NW 4th Street, Gainesville, Florida 32601, USA.
37. Stöhr, J.; Outka, D. A. Determination of Molecular Orientations on Surfaces from the Angular Dependence of near-Edge X-Ray-Absorption Fine-Structure Spectra. *Phys. Rev. B* **1987**, *36*, 7891–7905.
38. Diller, K.; Klappenberger, F.; Marschall, M.; Hermann, K.; Nefedov, A.; Wöll, C.; Barth, J. V. Self-Metalation of 2H-Tetraphenylporphyrin on Cu(111): An X-Ray Spectroscopy Study. *J. Chem. Phys.* **2012**, *136*, 014705.
39. Horcas, I.; Fernández, R.; Rodríguez, J. M.; Colchero, J.; Gómez-Herrero, J.; Baró, A. M. WSXM: A Software for Scanning Probe Microscopy and a Tool for Nanotechnology. *Rev. Sci. Instrum.* **2007**, *78*, 013705.
40. Ecija, D.; Vijayaraghavan, S.; Auwärter, W.; Joshi, S.; Seufert, K.; Aurisicchio, C.; Bonifazi, D.; Barth, J. V. Two-Dimensional Short-Range Disordered Crystalline Networks from Flexible Molecular Modules. *ACS Nano* **2012**, *6*, 4258–4265.
41. Krasnikov, S. A.; Beggan, J. P.; Sergeeva, N. N.; Senge, M. O.; Cafolla, A. A. Ni(II) Porphine Nanolines Grown on a Ag(111) Surface at Room Temperature. *Nanotechnology* **2009**, *20*, 135301–135301.
42. Beggan, J. P.; Krasnikov, S. A.; Sergeeva, N. N.; Senge, M. O.; Cafolla, A. A. Self-Assembly of Ni(II) Porphine Molecules on the Ag/Si(111)-Ag/Si(111)-(√3×√3)R30° Surface Studied by STM/STS and LEED. *J. Phys.: Condens. Matter* **2008**, *20*, 015003–015003.
43. Langner, A.; Hauschild, A.; Fahrenholz, S.; Sokolowski, M. Structural Properties of Tetracene Films on Ag(1 1 1) Investigated by SPA-LEED and TPD. *Surf. Sci.* **2005**, *574*, 153–165.
44. Barth, J. V.; Behm, R. J.; Ertl, G. Adsorption, Surface Restructuring and Alloy Formation in the Na/Au(111) System. *Surf. Sci.* **1995**, *341*, 62–91.
45. Diehl, R. D.; McGrath, R. Structural Studies of Alkali Metal Adsorption and Co-adsorption on Metal Surfaces. *Surf. Sci. Rep.* **1996**, *23*, 43–171.
46. Caragiu, M.; Finberg, S. Alkali Metal Adsorption on Graphite: A Review. *J. Phys.: Condens. Matter* **2005**, *17*, R995–R1024.
47. Gopakumar, T. G.; Brumme, T.; Kröger, I.; Toher, C.; Cuniberti, G.; Berndt, R. Coverage-Driven Electronic Decoupling of Fe-Phthalocyanine from a Ag(111) Substrate. *J. Phys. Chem. C* **2011**, *115*, 12173–12179.
48. Vijayaraghavan, S.; Ecija, D.; Auwärter, W.; Joshi, S.; Seufert, K.; Seitsonen, A. P.; Tashiro, K.; Barth, J. V. Selective Supramolecular Fullerene–Porphyrin Interactions and Switching in Surface-Confining C60–Ce(PPY)2 Dyads. *Nano Lett.* **2012**, *12*, 4077–4083.
49. Fernández-Torrente, I.; Franke, K. J.; Pascual, J. I. Spectroscopy of C60 Single Molecules: The Role of Screening on Energy Level Alignment. *J. Phys.: Condens. Matter* **2008**, *20*, 184001.
50. Repp, J.; Moresco, F.; Meyer, G.; Rieder, K.-H.; Hyldgaard, P.; Persson, M. Substrate Mediated Long-Range Oscillatory Interaction between Adatoms: Cu/Cu(111). *Phys. Rev. Lett.* **2000**, *85*, 2981–2984.
51. Knorr, N.; Brune, H.; Epple, M.; Hirstein, A.; Schneider, M. A.; Kern, K. Long-Range Adsorbate Interactions Mediated by a Two-Dimensional Electron Gas. *Phys. Rev. B* **2002**, *65*, 115420–115420.
52. Silly, F.; Pivetta, M.; Ternes, M.; Patthey, F.; Pelz, J. P.; Schneider, W.-D. Creation of an Atomic Superlattice by Immersing Metallic Adatoms in a Two-Dimensional Electron Sea. *Phys. Rev. Lett.* **2004**, *92*, 016101–016101.
53. Nanayakkara, S. U.; Sykes, E. C. H.; Fernández-Torres, L. C.; Blake, M. M.; Weiss, P. S. Long-Range Electronic Interactions at a High Temperature: Bromine Adatom Islands on Cu(111). *Phys. Rev. Lett.* **2007**, *98*, 206108–206108.
54. Stadtmüller, B.; Kröger, I.; Reinert, F.; Kumpf, C. Submonolayer Growth of CuPc on Noble Metal Surfaces. *Phys. Rev. B* **2011**, *83*, 085416.
55. Lau, K. H.; Kohn, W. Elastic Interaction of Two Atoms Adsorbed on a Solid Surface. *Surf. Sci.* **1977**, *65*, 607–618.
56. Brune, H.; Giovannini, M.; Bromann, K.; Kern, K. Self-Organized Growth of Nanostructure Arrays on Strain-Relief Patterns. *Nature* **1998**, *394*, 451–453.

57. Pohl, K.; Bartelt, M. C.; de la Figuera, J.; Bartelt, N. C.; Hrbek, J.; Hwang, R. Q. Identifying the Forces Responsible for Self-Organization of Nanostructures at Crystal Surfaces. *Nature* **1999**, *397*, 238–241.
58. Gonella, G.; Dai, H.-L.; Rockey, T. J. Tetracene Monolayer and Multilayer Thin Films on Ag(111): Substrate-Adsorbate Charge-Transfer Bonding and Inter-Adsorbate Interaction. *J. Phys. Chem. C* **2008**, *112*, 4696–4703.
59. Jeandupeux, O.; Bürgi, L.; Hirstein, A.; Brune, H.; Kern, K. Thermal Damping of Quantum Interference Patterns of Surface-State Electrons. *Phys. Rev. B* **1999**, *59*, 15926–15934.
60. Frenkel, D. The Simulation of Entropic Phase Transitions. *J. Phys.: Condens. Matter* **1994**, *6*, A71–A78.
61. Vanderbilt, D. Phase Segregation and Work-function Variations on Metal Surfaces: Spontaneous Formation of Periodic Domain Structures. *Surf. Sci.* **1992**, *268*, L300–L304.
62. Lau, K. H.; Kohn, W. Indirect Long-Range Oscillatory Interaction between Adsorbed Atoms. *Surf. Sci.* **1978**, *75*, 69–85.
63. Negulyaev, N. N.; Stepanyuk, V. S.; Niebergall, L.; Bruno, P.; Auwärter, W.; Pennec, Y.; Jahnz, G.; Barth, J. V. Effect of Strain Relaxations on Heteroepitaxial Metal-on-Metal Island Nucleation and Superlattice Formation: Fe on Cu(111). *Phys. Rev. B* **2009**, *79*, 195411.
64. Ali, M. E.; Sanyal, B.; Oppeneer, P. M. Tuning the Magnetic Interaction between Manganese Porphyrins and Ferromagnetic Co Substrate through Dedicated Control of the Adsorption. *J. Phys. Chem. C* **2009**, *113*, 14381–14383.
65. Häming, M.; Scheuermann, C.; Schöll, A.; Reinert, F.; Umbach, E. Coverage Dependent Organic-Metal Interaction Studied by High-Resolution Core Level Spectroscopy: SnPc (Sub)Monolayers on Ag(111). *J. Electron Spectrosc. Relat. Phenom.* **2009**, *174*, 59.
66. Heimel, G.; Duhm, S.; Salzmann, I.; Gerlach, A.; Strozecka, A.; Niederhausen, J.; Bürker, C.; Hosokai, T.; Fernandez-Torrente, I.; Schulze, G.; et al. Charged and Metallic Molecular Monolayers through Surface-Induced Aromatic Stabilization. *Nat. Chem.* **2013**, *5*, 187.
67. Comanici, K.; Buchner, F.; Flechtner, K.; Lukasczyk, T.; Gottfried, J. M.; Steinrück, H. P.; Marbach, H. Understanding the Contrast Mechanism in Scanning Tunneling Microscopy (STM) Images of an Intermixed Tetraphenylporphyrin Layer on Ag(111). *Langmuir* **2008**, *24*, 1987.